

FABRICATION AND CHARACTERIZATION OF NATURAL DYE-SENSITIZED SOLAR CELLS BASED ON PbS NANOSTRUCTURES

A. K. MISHRA*, S. SAHA

Department of Physics, Vidyasagar University, Paschim Midnapur, Pin-721102, West Bengal, India.

Natural dye-sensitized solar cells were fabricated based on differently shaped Lead Sulfide nanoparticles in a simple cost-effective way. The grown PbS nanoparticles were characterized by TEM, XRD, Optical Absorption, and Photoluminescence study. The natural dye-sensitized solar cell was fabricated using a kind of dye from *Clitoria ternatea* as a sensitizer. The current-voltage data of the dye-sensitized solar cell was taken under dark and light illuminated conditions. The dye-sensitized solar cell efficiency was measured and the ideality factor, fill factor were also found out. The open-circuit voltage and short circuit current density of the dye-sensitized solar devices based on three different shaped PbS nanoparticles are also obtained and compared.

(Received October 14, 2020; Accepted December 7, 2020)

Keywords: Nanostructure, Optical properties, Electrical characterization, Natural dye, Photovoltaic efficiency

1. Introduction

Nanostructures show properties dissimilar to their bulk structure so they are applicable in the various field of optoelectronic devices such as light-emitting diodes, photodetectors, gas sensors, biosensors, etc [1-5]. Semiconducting PbS nanoparticles are solution-processable and suitable material for solar cells due to their flexible optical and electrical properties [6-9]. PbS nanoparticles are used in photovoltaics for their properties like tunable band gap depending on particle size, large annihilation coefficient, and multiple exciton generation (MEG) with single-photon absorption [10-13]. It is the most vital challenge to fabricate simple low-cost photovoltaic devices with high efficiency. So photoelectrochemical cell is used to fulfill our high energy demand. Dye-Sensitized Solar cell (DSSC) has four sections such that (1) the dye-sensitized layer as an electrode to absorb solar energy (2) the transparent and conductive oxide layer to transfer charge from the electrode layer (3) graphite paint on ITO glass act as a counter electrode, (4) the redox electrolyte layer for reducing the level of energy supplied from the dye molecules [14-18]. Punnoose et al [19] prepared PbS/CdS/CdSe structured QDSSC by CBD and SILAR methods. They found that CBD produced a good uniform deposition of nanoparticles which provided high efficiency comparing with nanoparticles deposited by the SILAR method. Jianjun Tian et al [20] reported a PbS-quantum-dot-sensitized solar cell (QDSC) with a power conversion efficiency (PCE) of 4%. They further increased the performance of QDSCs, when the 30% deionized water of polysulfide electrolyte was replaced with methanol to improve the wettability and permeability of electrolytes in the TiO₂ film, which accelerated the redox couple diffusion in the electrolyte solution and improved charge transfer at the interfaces between photoanodes and electrolytes. They also improved the stability of PbS QDs in the electrolyte by methanol to reduce the charge recombination and prolong the electron lifetime. As a result, the PCE of QDSC was increased to 4.01%. Zhang et al. [21] obtained 5.11% efficiency using SILAR deposited 2PbS/CdS/CdSe on the TiO₂ layer (18 μm) which consisted of nanoparticles and microparticles. They observed a higher value of charge recombination resistance which clearly shows the reduction of recombination of photoelectrons at the interface. Umer Mehmood et al [22] replaced the expensive counter electrode material such as Platinum with low-cost lead sulfide (PbS). They found the results to show that PbS as a catalyst material showing good catalytic activity at the counter

* Corresponding author: anjanmishra2011@gmail.com

electrode of dye-sensitized solar cells (DSSCs). They fabricated DSSC with PbS showing the power-conversion-efficiency (PCE) of 4.71%, which was slightly lower than that of the Pt-based device (5.34%), under similar and optimal conditions. The p-type conductivity of PbS forms a junction between the PbS and the anode, by which photovoltage and fill factor are enlarged[23].

Three dye-sensitized solar cells (DSSC) are fabricated using different shaped PbS nanoparticles with natural dye molecules of *Clitoria ternatea*. Anthocyanin dye is collected from trees and it acts as a sensitizing agent to fabricate natural dye-sensitized solar cells. Dye-Sensitized Solar cell shows high efficiency due to the effective separation and transportation of the opposite charges generated in the dye molecules.

2. Experimental method

2.1. Sample grown and natural dye sensitizer preparation

PbS nanoparticles were synthesized using a chemical reduction method. Lead Chloride, Sulfur powder, and Sodium Borohydride were used to grow PbS nanoparticles using Ethylene Diamine (EDA) as a capping agent at 298K. To prepare a pure and apparent dye solution of *Clitoria ternatea*, fresh flowers of the plant were gathered from the garden. From these only 15 gm of the sample were taken separately using an electronic balance. After washing with distilled water properly, flowers were kept in a vacuum furnace for 4 hours at 40⁰C to be dry and dust-free. The flowers were crushed with a porcelain mortar and pestle. Then the crushed sample was kept in a beaker containing 60 ml ethanol at room temperature in a dark place. Finally, the solution was filtered with Whiteman filter paper. The pure and apparent dye solution was used as sensitizers for sensitizing PbS electrode to perform the photochemical effect.

2.2. Device fabrication

The dye-sensitized solar cells (DSSC) were based on three different shaped PbS nanoparticles and anthocyanin dye. Two ITO glass plates were kept in the beaker with ethanol and sonicated for 30 minutes using an ultrasonic bath. Teflon tape was used in ITO glass plates to give noncoated areas for electrical contact. 1.0gm of each PbS samples were added with 1 mL acetic acid (pH-3) and grinded in mortar for lump-free pestle. PbS paste was prepared. The conducting surface of the ITO sheet was covered with PbS paste by a doctor blade with adsorbed dye molecules as the sensitized photoanode. The active area of PbS film was 1 cm². A dried glass plate was kept in anthocyanin solution for 30 minutes. For the counter electrode, graphite is painted to the conducting surface of other ITO glass plates. Then two binder clips were used to sandwich the two electrodes together. Thereafter 0.5 mol of potassium iodide, 0.05 mol of iodine, 0.5 mol of acetic acid is used to prepare redox electrolyte solution. Three drops of redox electrolyte solution were injected into the interspaced between the cells and hence it served as a conductor to connect this electrode electrically.

2.3. Characterization

Optical absorption data of dyes are measured in the wavelength range of 200 nm–700 nm. The photoluminescence properties of anthocyanin dye are obtained in the range of 250 nm–700 nm. The DSSC device is fabricated with Anthocyanin dye which is collected from *Clitoria ternatea* flowers. The DSSCs, performance using anthocyanin dye as a sensitizer in ethanol solvent was determined by measuring the current density (J)-voltage (V) data under 100 mW cm⁻² light irradiation. The current density (J)-voltage (V) curves were plotted. The short circuit current density (JSC), open-circuit voltage (VOC), fill factor (FF), and power conversion efficiency (η) were measured for a DSSC sensitized by anthocyanin natural dye.

3. Results and discussion

3.1. Structural characterization

3.1.1. TEM picture study

The TEM images of three different shaped PbS Nanoparticles are shown in Fig. 1.

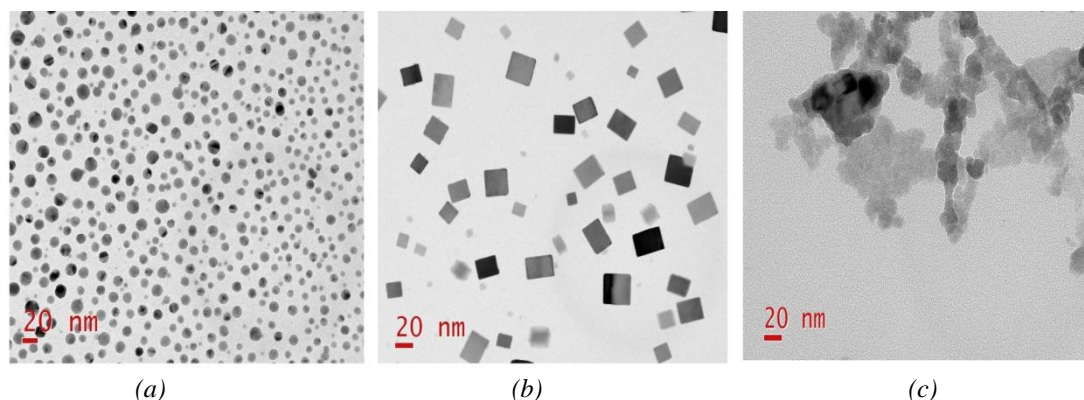


Fig. 1. The TEM images of (a) Spherical PbS (b) Cubic PbS NPs (c) chain-like PbS.

3.1.2. Powder X-ray diffraction study

The x-ray diffraction patterns of three different shaped PbS Nanoparticles are shown in Fig. 2.

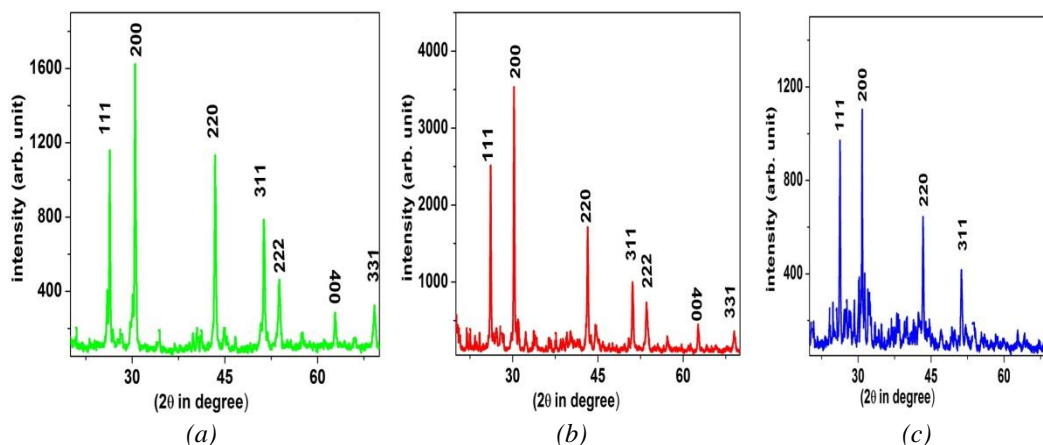


Fig. 2. The XRD patterns of (a) Spherical PbS (b) Cubic PbS NPs (c) chain-like PbS.

The crystalline phases of PbS samples are obtained by X-ray diffraction technique and grain size, preferred orientation, phase composition, and epitaxy are measured from this ideal method. The lattice parameter is also calculated from Bragg equation $2d_{hkl} \sin\theta = n\lambda$ where d_{hkl} is the interplanar distance of plane having Miller index (hkl) and θ is the Bragg angle. The wavelength of the incident radiation on powder crystal is λ and n is an integer. The XRD picture shows that various diffraction peaks at various 2θ value of 26.28, 30.48, 43.41, 51.26, 53.77, 62.8, 69.2 in degree corresponding to (111), (200), (220), (311), (222), (400), (331) plane respectively for spherical shaped PbS nanoparticles. The different value of 2θ for various diffraction peaks at 26.11, 30.12, 43.33, 51.11, 53.5, 62.56, 68.99 in degree corresponding to (111), (200), (220), (311), (222), (400), (331) respectively for cubic shaped PbS nanoparticles. Four diffraction peaks are seen for chain-like PbS at various 2θ values of 26.36, 30.8, 43.3, 51.1 in degree for (111), (200), (220), (311) planes respectively. This result of peak position is compared with standard JCPDS data. The face-centered cubic phase is identified. The average lattice parameter (a) value is obtained 0.59 nm by using

$$d = \frac{a}{\sqrt{h^2 + k^2 + l^2}}$$

The actual size of the PbS nanoparticles was measured from peak broadening in the X-ray diffraction lines. The average particle size (D) is calculated using the Scherrer equation

$$D = \frac{0.9\lambda}{\beta \cos\theta}$$

where λ is the wavelength of X-ray and β is the line broadening at half the maximum intensity (FWHM) in radians. 2θ is the Bragg angle.

The average particle size (D) is estimated as 9 nm, 14 nm, 19 nm for Spherical PbS, Cubic PbS NPs, chain-like PbS respectively.

3.2. Optical properties study

The optical absorbance spectra of PbS samples and the prepared dyes are shown in Fig. 3.

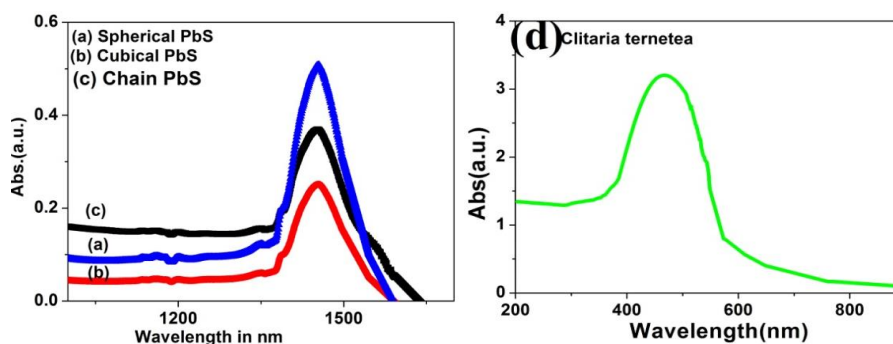


Fig. 3. The optical absorbance spectra of (a) Spherical PbS (b) Cubical PbS NPs (c) chain PbS and (d) natural anthocyanin dye.

The absorption between the ground state and excited states of the dye was found out by absorbance data. The absorption peak of natural dye was near 500 nm in ethanol medium and it was in the visible region. The natural dye has a core component as Anthocyanin which is responsible for absorption in the visible region.

The energy bandgap of PbS samples is shown in Fig. 4.

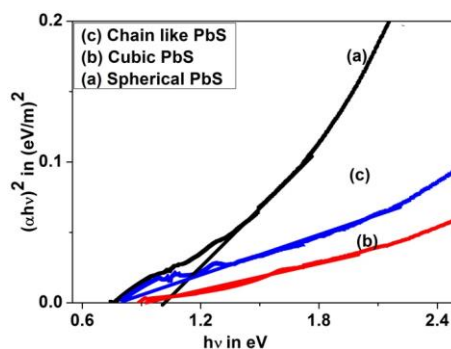


Fig. 4. The energy bandgap of (a) Spherical PbS (b) Cubical PbS NPs (c) chain-like PbS.

The bandgap of PbS nanomaterials is obtained using Tauc plot of $(\alpha hv)^2$ vs hv . Where hv is the energy of photon and absorption co-efficient (α) is determined from equation $\alpha = 2.303 \frac{A}{d}$, A is absorbance, d is the thickness of 1 cm for dispersed PbS sample which is taking in a cuvette. The linear portion of the graph is extrapolated to the energy axis and the bandgap energy is derived

from the intersection with the energy axis. The bandgap of spherical, cubical, and chain-like PbS nanomaterials are calculated as 1.02 eV, 0.95 eV, and 0.89 eV respectively.

The photoluminescence spectral of natural anthocyanin dye is shown in the Fig. 5

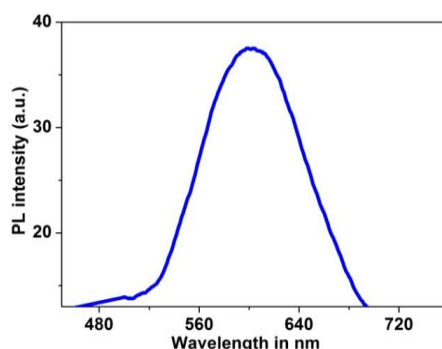


Fig. 5 The photoluminescence spectral of natural anthocyanin dye.

The photoluminescence spectra were obtained for excitation wavelength at 430 nm. The peak of the spectra was corresponding to wavelength 600 nm. Thus the peak of photoluminescence spectra was red-shifted at wavelength compared to the absorption peak as shown in optical absorption spectra. The emission peak mainly arises due to the transition from lower excited states to the ground state. Thus the excess absorbed energy was converted into heat for the transition from the higher excited state to the lower excited state.

3.3. Electric characterization of different DSSCs:

The schematic structure of the DSSC based on PbS nanomaterials is shown in Fig. 6.

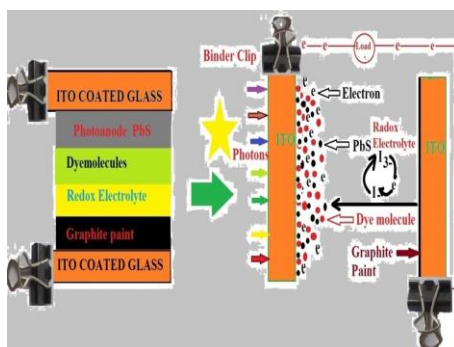


Fig. 6. The structure of the DSSC is based on PbS nanomaterials.

The current density-voltage data of the dye-sensitized solar cells based on three different shaped PbS nanoparticles were obtained in the dark and under the light. The photoelectric operational parameters were obtained from these characteristics. The open-circuit voltage, short circuit current was calculated from the current density (J) – voltage (V) graph. The maximum current density and the maximum voltage at the Maximum Power Point were calculated from the power density (P)- voltage(V) curves of DSSCs. The obtained J-V characteristics of the fabricated DSSCs based on three different shaped PbS nanomaterials under 100 mWcm^{-2} illumination is shown in figure 7.

The open-circuit voltage and short circuit current were measured when PbS paste coated side of ITO glass plate was irradiated with light. The fill factor and efficiency of DSSCs were obtained from J-V characteristics.

Current density (J) vs applied bias (V) characteristics of the fabricated DSSCs based on three different shaped PbS nanomaterials in ethanol solvent under dark and at fixed 100 mWcm^{-2} illuminations for natural dye in Fig. 7.

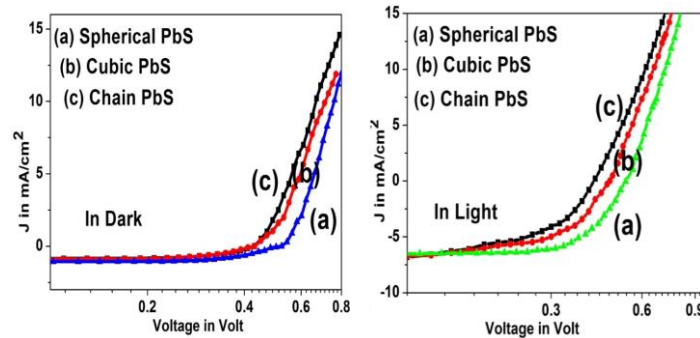


Fig. 7. The current density (J) vs applied bias (V) characteristics of the fabricated DSSCs based on (a) Spherical PbS (b) Cubic PbS NPs (c) Chain like PbS in ethanol solvent under dark and at fixed 100 mWcm^{-2} illuminations for natural dye.

The calculation was done from the relation of Fill factor by equation

$$FF = (J_m \times V_m) / (J_{sc} \times V_{oc}),$$

where J_m is maximum current density, and V_m is represented maximum voltage. Again J_{sc} is the short circuit current density and V_{oc} is the open-circuit voltage. The energy conversion efficiency (η) was measured by

$$\eta = FF \times (J_{sc} \times V_{oc}) / P_{in}$$

where P_{in} represents the incident power of radiation. V_{mp} , and J_{mp} is Voltage and current density at maximum power. V_{oc} , J_{sc} is open circuit voltage and short circuit current respectively. η is the efficiency of the cell. The fill factor was calculated from the J-V characteristics. Open circuit voltage of the Clitoria ternatea in ethanol solvent for spherical PbS, cubic PbS and bulk PbS are 0.54V, 0.47 V, and 0.42 V respectively. Short circuit current density of the Clitoria ternatea in ethanol solvent for spherical PbS, cubic PbS, and bulk PbS are 6.6 mA, 7 mA, and 7.8 mA respectively.

The ideality factor of the fabricated DSSCs based on three different shaped PbS nanoparticles is shown in Fig. 8.

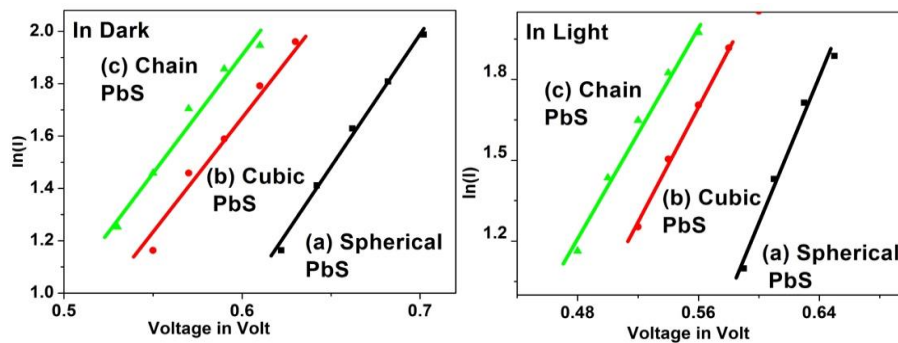


Fig. 8. The ideality factor of the fabricated DSSCs based on three different shaped PbS nanoparticles.

The larger value in the ideality factor is observed in three devices in dark to light illumination. This can be explained by surface states, the generation of electron holes, recombination, and barrier height. Atoms are disordered at the grain boundary and they may create some defects resulting in surface states. Barrier height also increases in smaller particles.

The power density of the fabricated DSSCs based on three different shaped PbS nanoparticles is shown in Fig. 9.

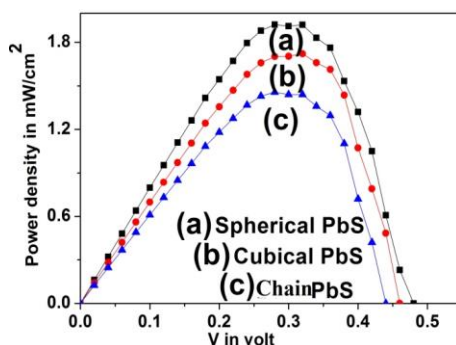


Fig. 9. The power density (P) – voltage (V) curves of prepared DSSCs based on (a) Spherical PbS (b) Cubical PbS NPs (c) chain PbS for different solvents and under different illumination of light intensity.

The maximum power efficiency ($\eta\%$) of prepared DSSCs based on spherical PbS nanoparticles and natural dye from the *Clitoria ternatea* flower of the plant was 1.91 in ethanol solvent. Different parameters of dye-sensitized solar cells based on three different shaped PbS nanoparticles obtained from J-V characteristics for natural dye and ethanol solvent at fixed illumination are shown in Table 1.

Table 1. Different characteristics value of a natural dye-sensitized solar cell based on PbS samples.

DSSCs based on	V_{oc} in Volt	J_{sc} (mA/cm^2)	FF (%)	Efficiency ($\eta\%$)	V_{max} in Volt	J_{max} in mA/cm^2	Ideality factor in dark	Ideality factor in light
Spherical PbS nanoparticles	0.54	6.6	50	1.92	0.33	5.8	4	2.8
Cubical PbS nanoparticles	0.47	7	46	1.49	0.3	5	4.2	3.8
Chain like PbS	0.42	7.8	40	1.26	0.28	4.5	4.4	4.1

3.4. Operation principle of DSSCs

There are two important steps in photo-voltaic devices to convert sunlight into electrical energy. The first step radiation absorption takes place with electron excitation and the second step involves charge carrier separation [31]. The way of radiation absorption and the separation of carriers in Dye-sensitized solar cells is quite different from solar cells based on a p-n junction. Both processes where radiation is absorbed and charge carriers are separated in classical solar cells by the semiconductor material itself. In the p-n junction, the charge separation is effected due to the potential barrier developed across the depletion layer [32]. On the other hand, light is absorbed by the dye molecules anchored to the semiconductor materials in DSSCs, and charge separation takes place at the dye-metal-oxide interface [33]. The preferred forward processes like photo-excitation processes, transportation processes, and regeneration of electrons in DSSC are described in the figure sequentially utilizing path 1-6 [34]. Under sunlight exposure, the dye molecules become photo-excited and inject electrons into the conduction band of the semiconducting metal

oxide. Then subsequently, the generation of the original configuration of the dye is due to electron donation from the electrolyte [35]. The quick generation of the dye by the electrolyte intercepts the recombination of the photoexcited electrons which ultimately flow towards the photo-anode. The electrolyte is generated at the counter electrode when the circuit is completed by an external load [36]. However, the efficiency of the cell is often reduced due to unfavorable recombinations of photo-excited electrons with the oxidized dye or tri-iodide [34].

The general mechanism of Dye-sensitized solar cells in presence of PbS nanoparticles is given below in Fig. 10.

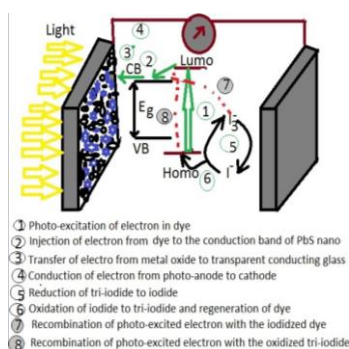


Fig. 10. General mechanism of Dye-sensitized solar cell in presence of PbS nanoparticles.

The recombination process of semiconductor nanoparticles with defect sites and surface states has a major responsibility in the charge transport and the efficiency is influenced by using surface modification processes of QDSSCs [24, 25]. In the QDSSCs, it is suppressed recombination which boosts the lifetime of electrons and efficiency [13].

The J-V plot shows power-driven out was increased in *Clitoria ternatea* due to anthocyanin in *Clitoria ternatea* [26]. Anthocyanins have OH & O⁻ group and have no carboxyl group to chemically bind with the PbS nano samples. Hence, the anthocyanin dye greatly improved the optical absorbance of the PbS nano samples. The molecular structure of the natural dye has OH & -O ligands. The molecular structure of the commercial dyes has mainly -COOH group to bind with semiconducting materials producing an ester and allow the free electron transfer to PbS nanoparticles conduction band to acquire a rapid electron-transport rate [27-28]. The performance of the natural dye of *Clitoria ternatea* flower of a plant treated with solvent as ethanol for two different shaped PbS nanoparticles and chain-like PbS are obtained.

4. Conclusions

Three different shaped PbS nanoparticles were synthesized by a simple cost-effective chemical method to apply in the dye-sensitized solar cell. The optical characteristics of natural dye anthocyanin were obtained from *Clitoria ternatea* flower extract. Dye-sensitized solar cells based on three different shaped PbS nanoparticles were constructed where the anthocyanin was used as a sensitizer. Power-driven out is maximum in *Clitoria ternatea* flower extract dye-sensitized solar cell based on spherical PbS nanoparticles and efficiency is 1.92. This efficiency gradually decreases with the increased size of PbS nanoparticles as well as a different shape. The greater efficiency of the device is due to the presence of anthocyanin as a dye that binds well spherical PbS nanoparticles. The many benefits of using dye-sensitized solar cells instead of traditional p-n junction silicon cells include lower purity requirements and abundance of component materials.

Acknowledgments

The authors are grateful to UGC & DST for their constant support through the SAP and FIST program to the Department of Physics, Vidyasagar University.

References

- [1] D. A. Hines, P. V. Kamat, *ACS Appl. Mater. Interfaces* **6**, 3041 (2014).
- [2] J. G. Radich, N. R. Peeples, P. K. Santra P. V. Kamat, *J. Phys. Chem. C* **118**, 16463 (2014).
- [3] Y. H. Lee, S. H. Im, J. A. Chang, J. H. Lee, S. I. Seok, *Org. Electron.* **13**, 975 (2012).
- [3] L. Hu, S. Huang, R. Patterson, J. E. Halpert, *J. Mater. Chem. C* **7**(15), 4497 (2019).
- [4] Z. Chen, Z. Zhang, J. Yang, W. Chen, Z. L. Teh, D. Wang, L. Yuan, J. Zhang, J. A. Stride, G. J. Conibear, R. J. Patterson, S. Huang, *J. Mater. Chem. C* **6**(37), 9861 (2018).
- [5] X. Zhang, V. A. Öberg, J. Du, J. Liu, E. M. J. Johansson, *Energy Environ. Sci.* **11**(2), 354 (2018).
- [6] Z. Tashan, M. Shalom, I. Hod, S. Rühle, S. Tirosh, A. Zaban, *J. Phys. Chem. C* **115**, 6162 (2011).
- [7] J. Tian, G. Cao, *Nano Rev.* **4**, 22578 (2013).
- [8] V. Gonzalez-Pedro, *Phys. Chem. Chem. Phys.* **15**, 13835 (2013).
- [9] A. Manjceevan, J. Bandara, *Sol Energy Mater Sol Cells* **147**, 157 (2016).
- [10] F. Cai, M. Pan, Y. Feng, G. Yan, Y. Zhang, Y. Zhao, *J Mod Transp* **25**, 52–57(2017).
- [11] F. Gao, Q. Chen, X. Zhang, H. Wang, T. Huang, L. Zhou, *Curr. Appl. Phys.* **18**, 546 (2018).
- [12] Y. Li, L. Wei, X. Chen, R. Zhang, X. Sui, Y. Chen, J. Jiao, L. Mei, *Nanoscale Res. Lett.* **8**(1), 1 (2013)
- [13] D. Punnoose, S. S. P. Kumar, H.W. Seo, M. Shiratani, A. E. Reddy, S. S. Rao, C. V. Thulasi-Varma, S. K. Kim, S. H. Chung, H. J. Kim, **40**, 3423 (2016).
- [14] L. Yu, Z. Li, Y. Liu, F. Cheng, S. Sun, *J. Mater. Sci. Mater. Electron.* **26**(4), 2286 (2015).
- [15] L. N. Van, H. T. Nguyen, H. V. Le, T. T. P. Nguyen, *J. Electron. Mater.* **46**, 274 (2017).
- [16] Y. Liu, J. Wang, *Thin Solid Films* **518**(24), e54 (2010).
- [17] N. Zhou, G. Chen, X. Zhang, L. Cheng, Y. Luo, D. Li, Q. Meng, *Electrochemistry Communications* **20**, 97 (2012).
- [18] L. Luo, H. Shen, W. Hu, Z. Yao, J. Li, D. Oron, N. Wang, H. Lin, *RSC Adv* **6**, 21156 (2016).
- [19] D. Punnoose, S. M. Suh, B.J. Kim, S. K. Kim, S. S. P. Kumar, S. S. Rao, C. V. Thulasi-Varma, A. E. Reddy, S. H. Chung, H. J. Kim, *J. Electroanalytical Chem.* **773**, 27 (2016).
- [20] J. Tian, T. Shen, X. Liu, C. Fei, L. Lv, G. Cao, *Scientific Reports* **6**, 23094 (2016).
- [21] X. Zhang, Y. Lin, J. Wu, J. Jing, B. Fang, *Opt. Commun.* **395**, 117 (2017).
- [22] U. Mehmooda, A. Ul Haq Khan, *Solar Energy* **193**, 1 (2019).
- [23] C. Y. Lin, C.Y. Teng, T. L. Li, Y. L. Lee, H. Teng, *Journal of Materials Chemistry A* **1**(4), 1155 (2013).
- [24] Z. Ren, J. Wang, Z. Pan, K. Zhao, H. Zhang, Y. Li, Y. Zhao, I. Mora-Sero, J. Bisquert, X. Zhong, *Chem. Mater.* **27**(24), 8398 (2015).
- [25] K. Zhao, Z. Pan, I. Mora-Sero, E. Canovas, H. Wang, S. Yong, X. Gong, J. Wang, M. Bonn, J. Bisquert, X. Zhong, *J. Am. Chem. Soc.* **137**(16), 5602 (2015).
- [26] P. S. Vankar, J. Srivastava, *International Journal of Food Engineering* **6**, 4 (2010).
- [27] H. J. Kim, Y. T. Bin, S. N. Karthick, K. V. Hemalatha, C. J. Raj, S. Venkatesan, S. Park, G. Vijayakumar, *Int. J. Electrochem. Sci.* **8**, 6734 (2013).
- [28] H. Chang, Y. J. Lo, *Solar Energy* **84**(10), 1833 (2010).
- [29] U. Mehmood, A. Al-Ahmed, M. Afzaal, A. S. Hakeem, S. Abdullahi Haladu, F. A. Al-Sulaiman, *IEEE Journal of Photovoltaics* **8**(2), 512 (2018).
- [30] L. Yuan, H. Michaels, R. Roy, M. B. Johansson, V. Öberg, A. Andruszkiewicz, E. M. J. Johansson, *ACS Applied Energy Materials*, 2020.
- [31] H. Z. Kafafi, R. J. Martín-Palma, A. F. Nogueira, D. M. Carroll, J. J. Pietron, I. D. W. Samuel, F. So, N. Tansu, L. Tsakalacos, *J. of Photonics for Energy* **5**,

- 050997 (2015).
- [32] K. G. Reddy, T. G. Deepak, G. S. Anjusree, S. Thomas, S. Vadukumpully, K. R. V. Subramanian, Shantikumar V. Nair, A. Sreekumaran Nair, *Phys. Chem. Chem. Phys.* **16**, 6838 (2014).
- [33] M. Borgwardt, M. Wilke, T. Kampen, S. Mähl, M. Xiao, L. Spiccia, K. M. Lange, I. Y. Kiyani, E. F. Aziz, *Sci Rep.* **6**, 24422 (2016).
- [34] D. Sengupta, P. Dasa, B. Mondal, K. Mukherjee, *Renewable, and Sustainable Energy Reviews* **60**, 356 (2016).
- [35] F. Bella, C. Gerbaldi, C. Barolo, M. Grätzel, *Chem. Soc. Rev.* **44**, 3431 (2015).
- [36] J. Wu, Z. Lan, J. Lin, M. Huang, Y. Huang, L. Fan, G. Luo, Y. Lin, Y. Xie, Y. Wei, *Chem. Soc. Rev.* **46**, 5975 (2017).
- [37] H. Yu, S. Zhang, H. Zhao, B. Xue, P. Liu, G. Will, *J. Phys. Chem. C* **113**, 16277 (2009).